NUMERICAL STUDY OF LOW VELOCITY FLUID FLOW THROUGH FRACTURED POROUS MEDIA

DUSTIN CRANDALL[1,2], GOODARZ AHMADI[1,2], KAMBIZ NAZRIDOUST[1], GRANT BROMHAL[2] AND DUANE SMITH[2]

[1]Mechanical and Aeronautical Engineering Dept., Clarkson University, Potsdam NY
[2]National Energy Technology Center, U.S. Department of Energy, Morgantown WV

Abstract

A set of simulations evaluating the effects of matrix permeability surrounding open fractures was performed. The fracture geometry was obtained from a CT scanned Berea sandstone fracture. Matrix permeabilities from 20md to 500md were studied and the resulting flow and pressure drop conditions are compared to previous simulations with impermeable fracture walls. For this range of geologic matrix permeabilities the predicted pressure drop associated with a given flow rate is shown to be reduced by approximately 40%. With this information an adjusted relationship between the flow rate and pressure loss over the fractures is given that accounts for the fracture characteristics and fluid flow. This relationship utilizes an approximate friction factor to account for the fracture geometry, similar to the cubic law.

1. INTRODUCTION

Understanding the physics of fluid flow through fractures is important for assessing and planning subsurface activities. These include the recovery of oil and natural gas, nuclear waste repositories, carbon dioxide sequestration in geologic media and water resource analysis. The inherent high permeability of open fractures lends itself to faster movement of fluids as compared to the majority of geologic media. Numerous experimental studies of flow through fractures were reported in the literature. These include flow through single fractures [Konzuk and Kueper, 2004], flow in intersecting fractures [Johnson and Brown, 2001] and flow in fractured porous media [Billstein et al., 1999]. Approximations of these fracture flow relations are used in reservoir scale models.

In this study the flow through a fracture is analyzed and the pressure drops for a range of flow rates over the fracture length were evaluated for four fracture sections. The permeability of the matrix surrounding the fracture was varied in order to assess its impact on the flow through geologic media of different properties.

For this study, the Navier-Stokes equation was solved to account for the viscous fluid flow using FLUENT^{TM}, a commercial CFD software. For fixed flow rates at the fracture inlet, the pressure contours in the fracture and within the surrounding permeable matrix were computed. An empirical equation for a fracture friction factor was obtained that could be useful for application to fractured reservoir simulation.

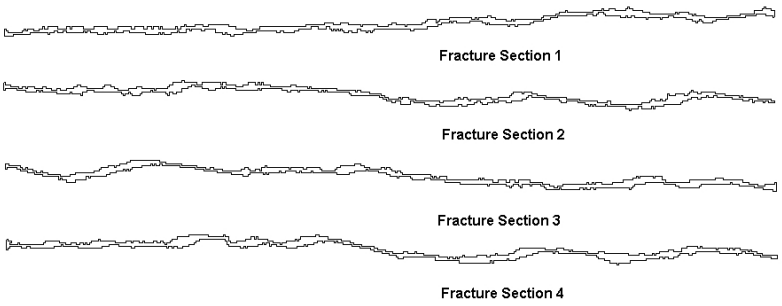

FIGURE 1. Two-dimensional fracture sections studied.

1.1. **Fracture Model.** The fracture geometry used in this study was obtained by Li et al. [2005] by utilizing a modified Brazilian method on a 2.64 cm diameter, 10.15 cm long core of Berea sandstone. The modification was the use of a flat plates on the top and bottom of the sample to induce the fracture in the core. The fracture was assumed to be generated with nearly identical stress distribution as with the standard Brazilian method [Chen et al., 1998]. Their CT scanning of this fracture provided the digitalized form of the geometry. The original three dimensional binary data was cleaned to remove unconnected regions of low porosity sandstone that were recognized by the scanner. This cleaned binary data was converted into a CAD recognizable geometry with the use of an in-house code.

Four two-dimensional fracture 'traces' were identified from this three-dimensional set. These 'traces' were used due to their lack of closed throat regions, thus enabling two-dimensional modeling over the entire fracture length. The fracture sections studied are shown in Figure 1. A number of geometric characteristics of these traces were analyzed. These included the tortuosity of the fluid path within the open sections and the distribution of aperture sizes.

Tortuosity (Θ) was defined as the percentage increase in distance traveled by fluids flowing through a fracture due to the roughness, asperities and aperture distribution [Tsang, 1984, Brown, 1989, Zimmerman et al., 1992, Brown et al., 1998]. Here Θ is defined as in Nazridoust et al. [2006],

$$\Theta = \frac{L_{flow}}{L} - 1 \tag{1}$$

where L_{flow} is the length that the fluid travels and L is the length of the fracture. While this may be an abstract quantity to measure in physical situations, the use of FLUENT^{TM} software enables a direct measurement via the length of flow pathlines and the overall length of the fracture. For the sections studied Θ varied from 3.4% to 4.6%, corresponding to Sections 1 and 4, respectively. These values are lower than Θ's that have been reported by Brown [1989]. This is perhaps due to the two-dimensional realization of the fracture in this study.

The throat distribution over the open sections was measured and as well. The average throat size of the four sections was found to be $0.593mm$ ($0.0233in$), with minimum and maximum throats of $0.240mm$ and $1.44mm$. This is similar to aperture distributions reported by Lanaro [2000] for an experimental sample of basic gneiss. Figure 2 shows

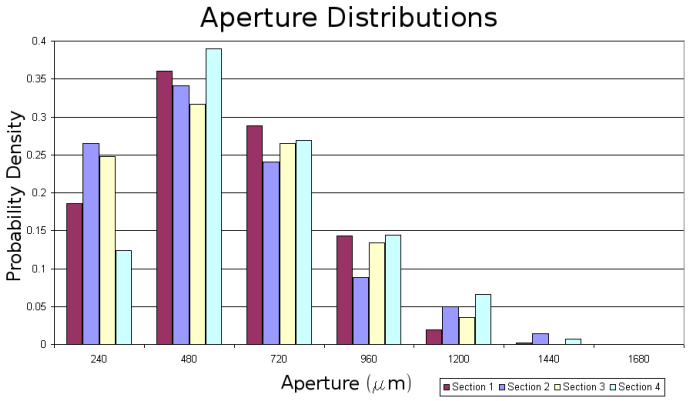

FIGURE 2. Aperture distribution of fracture sections.

the distributions of all four sections, with the aperture sizes given in microns. The standard deviation (σ) of the apertures was calculated for each section as well, varying from $0.293mm$ for Section 4 to $0.303mm$ for Section 3.

1.2. **Assumptions.** Single phase flows through fractures were studied. Flows of air with a density, $\rho = 1.225\frac{kg}{m^3}$ and viscosity, $\mu = 1.8 \cdot 10^{-5}\frac{kg}{m \cdot s}$ and water with $\rho = 998\frac{kg}{m^3}$ and $\mu = 1 \cdot 10^{-3}\frac{kg}{m \cdot s}$ within the fractures were studied. While the majority of subsurface flow involves multiple fluids and interconnected fracture networks, the analysis of single phase fluid motion through individual fractures provides considerable insight into the processes involved. This is of importance for proper engineering estimates in geologic activities.

The porous matrix was assumed to have homogeneous properties over the flow domain studied. A porosity of 30% was used for the matrix in all simulations. The matrix was also assumed to be non-deforming, which is acceptable at the low pressure differences developed during the simulations.

2. MODELING OF FRACTURE FLOW

2.1. **Traditional Approximations.** In discrete fracture models, the use of parallel plate flow approximations has been common. Accordingly, for laminar flows

$$Q = \frac{1}{12}\frac{\Delta P h^3}{\mu L} \tag{2}$$

where Q is the flow rate, ΔP is the pressure drop, L is the length of the plates and h is the distance between the plates. Equation (2) is commonly known as the cubic law. Multiple variations of this relationship have been proposed, including locally applied cubic relations [Oron and Berkowitz, 1998], h defined as an apparent fracture aperture [Konzuk and Kueper, 2004], h based upon the average aperture height [McKoy and Sams, 1997] and combinations of these approaches.

An alternative to the typical methods of modeling fluid flow in fractures was proposed by Nazridoust et al. [2006] in which a new friction factor relationship for fractures was proposed. Friction factors (f) have been used for over a century to account for fluid flow losses in rough pipes, and are often tabulated in various forms like the Moody diagram.

Equation (3) is a common formula used to define the friction factor,

$$f = \frac{2\Delta P \cdot \bar{H}}{\rho L V^2} \tag{3}$$

where V is the average flow velocity and H is the aperture length value. This relates the fluid motion to the geometric parameters of the flow, the fluid properties and the associated pressure drops. When the matrix is impervious, Nazridoust et al. [2006] suggested,

$$f = \frac{123}{Re_{\bar{H}}} \left(1 + 0.12 Re_{\bar{H}}^{0.687}\right) \tag{4}$$

where $Re_{\bar{H}}$ is the Reynolds number

$$Re_{\bar{H}} = \frac{Q}{\nu} \tag{5}$$

ν is the kinematic viscosity and $\bar{H} = H_{avg} - \sigma$ is the length scale of importance (due to large pressure losses through smaller apertures). Equating (3) and (4) allows one to solve for a pressure drop over a length of fracture with known statistical properties. That is,

$$\Delta P = Q \frac{\mu L(1+\Theta)}{\bar{H}^3} \left(61.5 + 7.38 \left(Re_{\bar{H}}\right)^{0.687}\right) \tag{6}$$

2.2. **Governing Equations.** This study differs from the majority of previously published material in that the full Navier-Stokes equations for conservation of mass and fluid momentum are solved to accurately model the fluid flow throughout the computational domain. Mass conservation is described by

$$\frac{\partial \rho}{\partial t} + \nabla \cdot (\rho \vec{v}) = 0 \tag{7}$$

Balance of momentum is given as,

$$\frac{\partial}{\partial t}(\rho \vec{v}) + \nabla \cdot (\rho \vec{v} \vec{v}) = -\nabla p + \nabla \cdot (\bar{\bar{\tau}}) + \rho \vec{g} + \vec{S} \tag{8}$$

where $\vec{v}$ is the velocity vector, $\vec{g}$ is the acceleration due to gravity, $\vec{S}$ is the applied source terms (porous approximation in matrix; zero within fracture domain) and $\bar{\bar{\tau}}$ is the stress tensor, given by

$$\bar{\bar{\tau}} = \mu \left[(\nabla \vec{v} + \nabla \vec{v}^T) - \frac{2}{3} \nabla \cdot \vec{v} I \right] \tag{9}$$

where I is the identity matrix. For the fracture domain $\vec{S}$ is zero. For the matrix region an source term is described by the combination of a Darcy loss term and an inertial loss term,

$$S_i = -\left(\sum_{j=1}^{3} D_{ij} \mu v_j + \sum_{j=1}^{3} C_{ij} \frac{1}{2} \rho v_{mag} v_j \right) \tag{10}$$

where D_{ij} is the directional matrix of viscous losses and C_{ij} is the directional matrix of inertial losses. For this study a homogenous porous media was assumed and low velocity fluid was examined, hence (10) reduces to the following [FLUENT Inc., 2005]

$$S_i = -\left(\frac{\mu}{k} v_i \right) \tag{11}$$

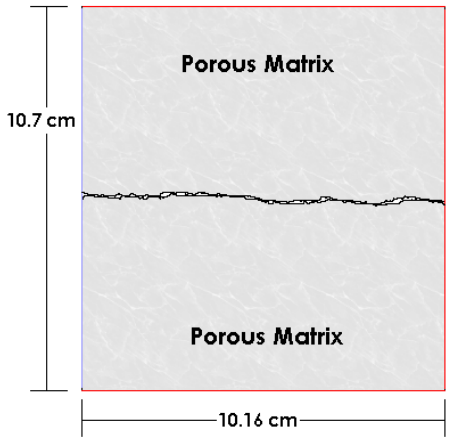

FIGURE 3. Flow domain of fracture Section 2 and surrounding porous matrix.

where k is the permeability.

3. COMPUTATIONAL PARAMETERS

3.1. **Computational Domain.** A $10.16cm$ by $10.7cm$ flow domain was generated for each fracture section, as shown for Section 2 in Figure 3. Velocity inlets were specified on the left side of the domain with a set velocity at the fracture opening and a flow rate of zero set for the surrounding matrix. Outflow conditions on the top, bottom and right side were used in order to calculate the pressure and velocity in the computational domain as well as at these edges. The porous media conditions of (10) were applied to the porous matrix.

A structured quadrilateral mesh with $20\mu m$ edges was applied to the fracture and its immediate surrounding media. An unstructured triangular mesh was used for the media further away from the fracture. The average number of grid cells per domain was about $3.3 \cdot 10^6$, with the highest grid resolution in the regions including and directly surrounding the fracture. The two dimensional segregated solver was used under laminar flow assumption. The standard pressure discretization scheme was used along with the 2^{nd} Order Upwind scheme for momentum.

3.2. **Parameters altered for study.** For all four fracture sections the flow rate was varied from 0.312 to 21.6 $\frac{mm^2}{s}$ in order to directly relate the results to the previous work of Nazridoust et al. [2006]. The permeability of the porous media was varied from 20md to 500md to cover the permeabilities commonly found in subsurface geologic material. A total of 46 cases were run for each fluid; water and air.

4. RESULTS

The eight log-log plots of Figures 4 and 5 show the relationship between flow rate and pressure drop over the four sections for air and water flow. These figures show that the pressure drop increases linearly with the flow rate. As can be seen the slope is the same for the cases with porous media and impermeable walls ($k = 0$). For the studied sections the calculated pressure loss of the flows is approximately 40% less than the associated

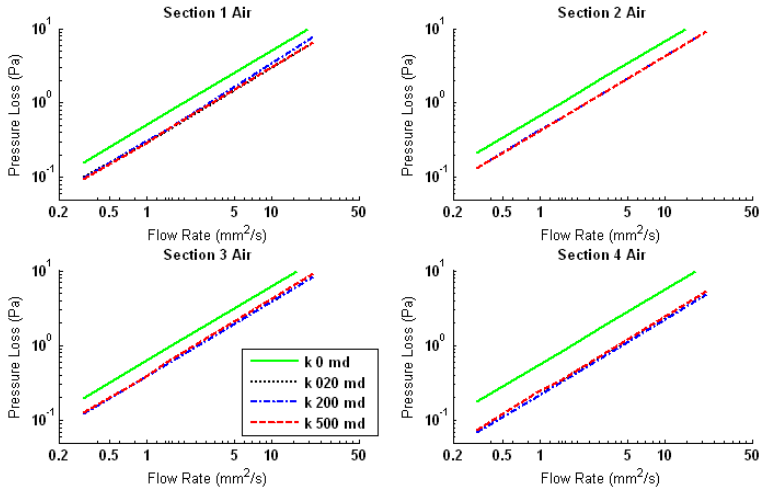

FIGURE 4. Pressure loss calculated for range of flow rates, air.

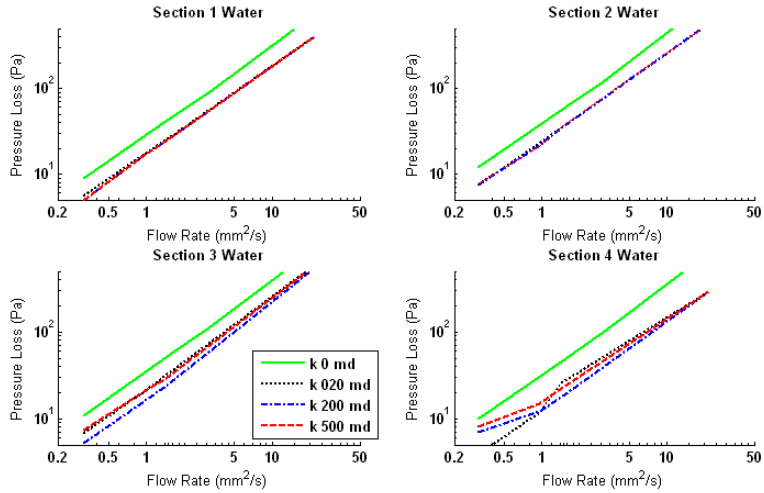

FIGURE 5. Pressure loss calculated for range of flow rates, water.

pressure drop for an impermeable matrix. The greatest variation from this is seen by the flow-pressure relationship observed in Section 4, which is approximately 60% less than the impermeable case. Variations of less than 1% change in pressure drop are seen for the three permeable cases.

Comparing the results for the fracture friction factor given by Nazridhoust et al. [2006] with the results shown in Figures 4 and 5 it is found that the inclusion of porous media surrounding the fracture causes a decrease in the pressure drop, roughly equivalent to 40% of the originally proposed solution. Hence a revised expression for the friction fracture, f, is proposed for situations where the permeability of the matrix surrounding a fracture needs to be accounted for. That is,

$$f = \frac{91}{Re_{\bar{H}}} \left(1 + 0.12 Re_{\bar{H}}^{0.687}\right) \tag{12}$$

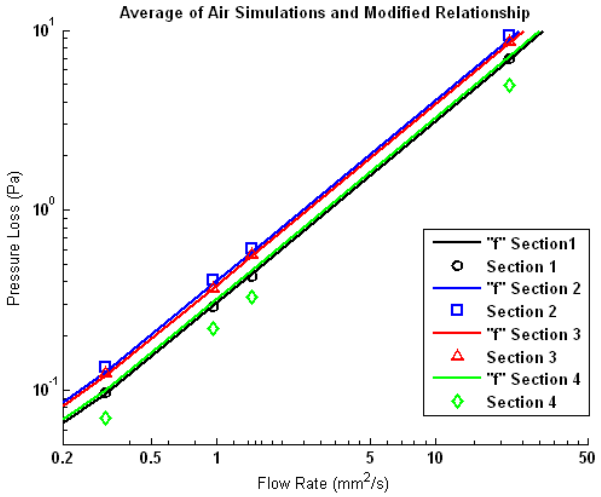

FIGURE 6. Comparison of revised f relationship and air simulation results.

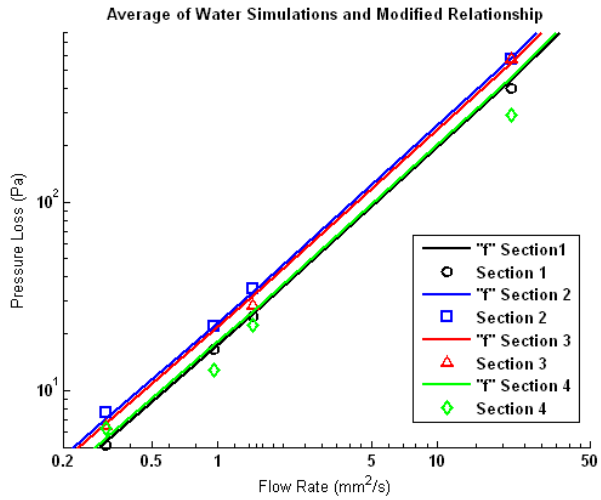

FIGURE 7. Comparison of revised f relationship and water simulation results.

Equation (12) is in good agreement with the simulated values. A plot of this altered f relationship is shown in Figure 6 for the air flow cases and in Figure 7 for the water cases. The average values of all pressure drops at set flows are used for comparison due to the small variation seen between these cases, which gives credence to the use of a single relationship for flow approximations in open fractures when the permeability of the matrix is assumed to be significant. An average difference between the friction factor relationship and the Navier-Stokes solutions is less than 5% for the average of sections 1,2 and 3 for the water case and less than 3% for the air cases. Section 4 varies the most from both the previously defined f relationship and the new formulation. The reliance of the pressure-flow relationship on the smallest apertures within the fracture is confirmed by the agreement of the calculated data to the inverse of $Re_{\bar{H}}$ at small flow rates.

5. CONCLUSIONS

By utilizing the Navier-Stokes and the mass conservation equations, it was shown that the presence of a permeable matrix surrounding an open fracture reduces the pressure drop. Comparison with previously simulated fracture flows that used impermeable fracture walls shows that the matrix permeability roughly reduces the pressure drop by 40%. The friction factor proposed by Nazridhoust et al. [2006] was modified to account for the effect of matrix permeability.

References

Billstein, M., U. Svensson and N. Johansson (1999) Application and validation of a numerical model of flow through embankment dams with fractures: comparisons with experimental data, *Can. Geotech. J.*, *37*, 651-659.

Brown, S. (1989) Transport of Fluid and Elecric Current Through a Single Fracture, *J. Geophys. Res.*, *94*(B7), 9429-9438.

Brown, S., A. Caprihan and R. Hardy (1998) Experimental observation of fluid flow channels in a single fracture, *J. Geophys. Res.*,*103*(B3), 5125-5132.

Chen, C.-S., E. Pan and B. Amadei (1998), Determination of deformability and tensile strength of anisotropic rock using Brazilian Tests, *Int. J. Rock Mech. Min. Sci.*, *35*(1), 43-61.

Fluent Inc. (2005) FLUENT 6.2 User's Manual, Chapter 7, Section 19, 104-124.

Johnson, J. and S. Brown (2001) Experimental mixing variablity in intersecting natural fractures, *Geophys. Res. Let.*, *28*(22), 4303-4306.

Konzuk, J.S. and B.H. Kueper (2004) Evaluation of cubic law based models describing single-phase flow through a rough-walled fracture, *Wat. Resour. Res.*, *40*, doi:10.1029/2003WR002356.

Lanaro, F. (2000) A random field model for surface roughness of rock fractures, *Int. J. Mech. Min. Sci.*, *37*, 1195-1210.

Li, G., Z.T. Karpyn, P.M. Halleck and A.S. Grader (2005) Numerical Simulation of a CT-Scanned Counter-Current Flow Experiment, *Trans. Por. Media*, *60*, 225-240.

McKoy, M.L. and W.N. Sams (1997) Tight gas reservior simulation: modeling discrete irregular strata-bound fracture networks and metwork flow, including dynamic rechange from the matrix (1997) Presented at 1997 DOE Natural Gas Conference, Houston, TX. March 24-27, Paper P17.

Nazridoust, K., G. Ahmadi and D.H. Smith (2006) A New Friction Factor Correlation for Laminar, Single Phase Flows through Rock Fractures, *J. Hydro.*, In Press.

Oron, A.P. and B. Berkowitz (1998) Flow in Fractures: the local cubic law assumption reexamined, *Wat. Resour. Res.*, *34*, 2811-2825.

Tsang, Y.W. (1984) Effect of Tortuosity on Fluid Flow Through a Single Fracture, *Wat. Resources Res.*, 4W0827, 1209-1215.

Zimmerman, R.W., D.-W. Chen and N.G.W. Cook (1992) The effect of contact area on the permeability of fractures, *J. of Hydro.*, *139*, 79-96.